Quantum dot $PbS_{0.9}Se_{0.1}/TiO_2$ heterojunction solar cells

2012 Nanotechnology 23 405401

(http://iopscience.iop.org/0957-4484/23/40/405401)

Nanotechnology **23** (2012) 405401 (7pp) doi:10.1088/0957-4484/23/40/405401

Quantum dot $PbS_{0.9}Se_{0.1}/TiO_2$ heterojunction solar cells

Guangmei Zhai[1,2], Carena P Church[2], Alison J Breeze[3], Daoli Zhang[1], Glenn B Alers[2] and Sue A Carter[2]

[1] Department of Electronic Science and Technology, Huazhong University of Science and Technology, Wuhan 430074, People's Republic of China
[2] Department of Physics, University of California, Santa Cruz, CA 95064, USA
[3] Solexant Corporation, San Jose, CA 95131, USA

E-mail: sacarter@ucsc.edu

Received 25 May 2012, in final form 8 August 2012
Published 20 September 2012
Online at stacks.iop.org/Nano/23/405401

Abstract

We report on photovoltaic cells based on ternary $PbS_{0.9}Se_{0.1}$ quantum dots utilizing a heterojunction type device configuration. The best device shows an AM 1.5 power conversion efficiency of 4.25%. Furthermore, this ternary PbS_xSe_{1-x} quantum dot heterojunction device has a peak external quantum efficiency above 100% at 2.76 eV, approximately 2.7× the bandgap energy. The ternary quantum dots combine the higher short circuit currents of the binary PbSe system with the higher open circuit voltages of the binary PbS system.

S Online supplementary data available from stacks.iop.org/Nano/23/405401/mmedia

(Some figures may appear in colour only in the online journal)

Photovoltaic devices with active layers consisting of films formed by colloidal IV–VI quantum dots (QDs) have attracted considerable attention, due to their low-cost solution processability, desirable electrical properties [1], high photoactivity in the near-infrared spectral region and potential ultrahigh conversion efficiencies via multiple exciton generation (MEG) [2–6]. So far, Schottky and heterojunction solar cells based on binary IV–VI QDs, such as PbS and PbSe, have been intensely investigated and great progress in device fabrication and performance has been made. However, solar cells employing ternary PbS_xSe_{1-x} QDs have not received as much attention, even though it has been demonstrated that PbS_xSe_{1-x} QDs can maintain the advantages of both binary compound counterparts [7]. The few papers [7, 8] on ternary PbS_xSe_{1-x} QD solar cells demonstrate an efficiency of ∼3.4% in a Schottky junction device. However, Schottky junction solar cells have several drawbacks that potentially impede further improvement of device performance [9, 10]. Heterojunction solar cells can overcome the limitations of Schottky architecture by introducing a charge-dissociating junction formed between QD films and transparent metal oxide layers, such as TiO_2 and ZnO. Moreover, only heterojunction structures have shown MEG in working solar cell devices.

MEG in quantum dot systems has been mainly observed to date in colloidal QD solutions [2, 3, 11] and films [12–14] via spectroscopic measurements. An absorbed photon-to-current efficiency greater than 100%, namely an internal quantum efficiency >100%, has recently been reported in a photoelectrochemical cell composed of a monolayer of PbS QDs chemically bound to single crystal TiO_2 [15]. The sensitivity of QD devices to environmental conditions [16] and significant optical interference and scattering of multilayer stack in devices implies that the only conclusive measurement of MEG is an external quantum efficiency (EQE), namely the number of electrons collected divided by the number of photons incident on the surface of the device, above 100% in working solar cells. Despite some Schottky junction devices showing high current densities (J_{sc}) [17], MEG has not been shown to exist in these devices. The NREL group has very recently reported a peak EQE exceeding 100% in ZnO/PbSe QD devices [18], in which PbSe QDs were treated by 1,2-ethanedithiol (EDT) and hydrazine sequentially, showing conclusive evidence for MEG in QD heterojunctions. Nonetheless, these results largely occurred at energies above 2.8 eV, where solar intensities are too low to take advantage of MEG to achieve higher J_{sc}.

In this paper we report on the fabrication and characterization of heterojunction solar cells consisting of a TiO_2 window layer and a ternary $PbS_{0.9}Se_{0.1}$ QD layer. We show that both high photocurrents and reasonable open circuit voltages (V_{oc}) are achieved simultaneously in such donor–acceptor structures, representing an improvement of about 30% compared to its former Schottky counterpart [7]. Moreover, we observe a peak external quantum efficiency above 100% in ternary $PbS_{0.9}Se_{0.1}$ QD heterojunction devices solely treated with EDT, suggesting that multiple exciton generation (MEG) can still exist even in the absence of hydrazine [13] by using ternary QDs and optimizing device fabrication.

Lead oxide (PbO, 99.999%), selenium (99.99%), oleic acid (OA, 90%), diphenylphosphine (DPP, 98%), bis(trimethylsilyl) sulfide (TMS_2-S, synthesis grade), 1-octadecene (ODE, 90%), titanium (IV) ethoxide (technical grade), anhydrous solvents were purchased from Sigma-Aldrich and used as received. Trioctylphosphine (TOP, >96%), 1,2-ethanedithiol (EDT, >95%) and TiO_2 nanoparticle paste were acquired from Cytec, Alfa Aesar, and Solaronix, respectively. Standard air-free techniques were used throughout synthesis and purification process. Ternary PbS_xSe_{1-x} QDs, provided by Solexant, were synthesized using a variation on a literature route [7]. Briefly, 1.38 g of PbO, 4.2 g of OA, and 30 g of ODE were mixed in a three-necked flask and then degassed and heated at 150 °C for one hour to dissolve the PbO and dry the solution. The temperature was then lowered to 118°C, and a mixture of 1 M TOP/Se solution (2.1 ml), TMS_2-S (189 μl), DPP (120 mg), and ODE (3.6 ml) was rapidly injected. The total amount of Se and S precursor was 3 mmol, with the ratio of 7:3. The reaction was quenched after 20 s by injecting 20 ml of room-temperature hexane to halt the nanocrystal growth. The QDs were purified with isopropanol and finally dispersed in octane to achieve a concentration of 50–100 mg ml^{-1}.

The TiO_2 sol–gel was prepared using titanium ethoxide as precursor by the standard procedure described previously [19]. The TiO_2 sol–gel and nanoparticle paste were spin-coated onto a cleaned glass substrate with pre-patterned indium tin oxide (ITO) electrodes of 150 nm thickness (Thin Film Devices, Anaheim) sequentially. Both TiO_2 sol–gel (∼75–100 nm thick) and nanoparticle (∼225–250 nm thick) layers were sintered at 450 °C for 30 min in air to improve conductivity. The PbS_xSe_{1-x} ternary QD film was deposited onto the TiO_2 film via multilayer spin-coating QD ink in a nitrogen-filled glove box. Each PbS_xSe_{1-x} layer was treated briefly by immersing the substrate into EDT in acetonitrile solution (1%, v/v) for around 15 s to increase electronic coupling between the QDs. The thickness of QD film was controlled by adjusting the spin-coating speed, iteration times and concentration of QD ink. Finally, 100 nm of gold contact was thermally evaporated under high vacuum (10^{-5}–10^{-6} Torr) at a rate of 0.6 Å s^{-1}. The area of each device formed is 0.03 cm^2.

All device characterizations were carried out in a nitrogen-filled glove box, at an oxygen partial pressure below 50 ppm. Current-density–voltage (J–V) curves were taken using a calibrated solar simulator and a Keithley 2400 source meter, and EQE curves were taken using the solar simulator coupled into an Oriel monochromator. In monochromatic measurement experiments, diode lasers of 405 and 447 nm were used as light sources. For light intensity dependent experiments, a set of neutral density filters (Newport) were used to adjust the intensity of the light source. A Shimadzu UV-3101PC UV–vis–NIR spectrometer was used to measure the absorption spectra of ternary PbS_xSe_{1-x} QD solution. Optical properties of ternary QD films were measured via a StellarNet TF-C-UVIS-SRN dual spectrometer. Transmission electron microscope (TEM) images were taken using a Philips CM200UT electron microscope. The topography and thickness of PbS_xSe_{1-x} QD film were obtained by an atomic force microscope (AFM) operating in tapping mode. A Hitachi S-4800 II field emission scanning electron microscope was employed to observe the cross section of the device and confirm the thickness of each layer. Energy dispersive x-ray spectroscopy (EDX) measurements were taken via an EDX spectrometer attached to the HR-SEM.

Figure 1(a) shows TEM images of PbS_xSe_{1-x} QDs employed in this work. These images reveal the formation of quasi-spherical nanocrystals with an average diameter between 3.4 and 3.5 nm. The ensemble of QDs in the images exhibited that ternary nanocrystals have a diameter distribution of <15% and were self-organized into a hexagonal array. EDX results indicate that the ratio of S to Pb, namely x, is 0.90 ± 0.05. Therefore, our QDs are mainly comprised of $PbS_{0.9}Se_{0.1}$, which we use from here on. Figure 1(b) shows an AFM topography image of a $PbS_{0.9}Se_{0.1}$ QD film treated with EDT on a glass substrate. The surface of ternary QD film has a root mean square roughness of 4 nm. The room temperature absorption (blue dashed line) of $PbS_{0.9}Se_{0.1}$ QDs capped with oleic acid molecules is shown in figure 1(c). The spectrum exhibits an obvious sharp absorption peak at a wavelength of 1076 nm due to the strong quantum confinement effect. The half-width at full maximum is 80 nm in the absorption data, which suggests a variance of ±0.1 eV for the band gap of the quantum dot. The red solid line in figure 1(d) represents the absorption of spin-cast ternary QD film treated with EDT. Both absorption spectra appear to be nearly identical in shape, except for the red-shift of the first exciton in the EDT treated film by around 60 meV, likely due to strengthened dipole-induced dipole interactions and wavefunction delocalization [20]. According to the relationship between nanocrystal diameter and absorption band gap for binary PbS [21] and PbSe [22] QDs reported previously, the obtained x value of ternary PbS_xSe_{1-x} QDs would be approximately 0.8 ± 0.1. This value is lower than what is suggested by our EDX measurements, but consistent with the relatively large error bars for both measurements.

The structure and cross-sectional HR-SEM image of a photovoltaic device incorporating n-type TiO_2 sol–gel and nanoparticle layers and a p-type ternary $PbS_{0.9}Se_{0.1}$ QD layer are presented in figure 2. We studied the effects of ternary PbS_xSe_{1-x} QD film thickness on solar cell performance. We note that the thickness of $PbS_{0.9}Se_{0.1}$ QD

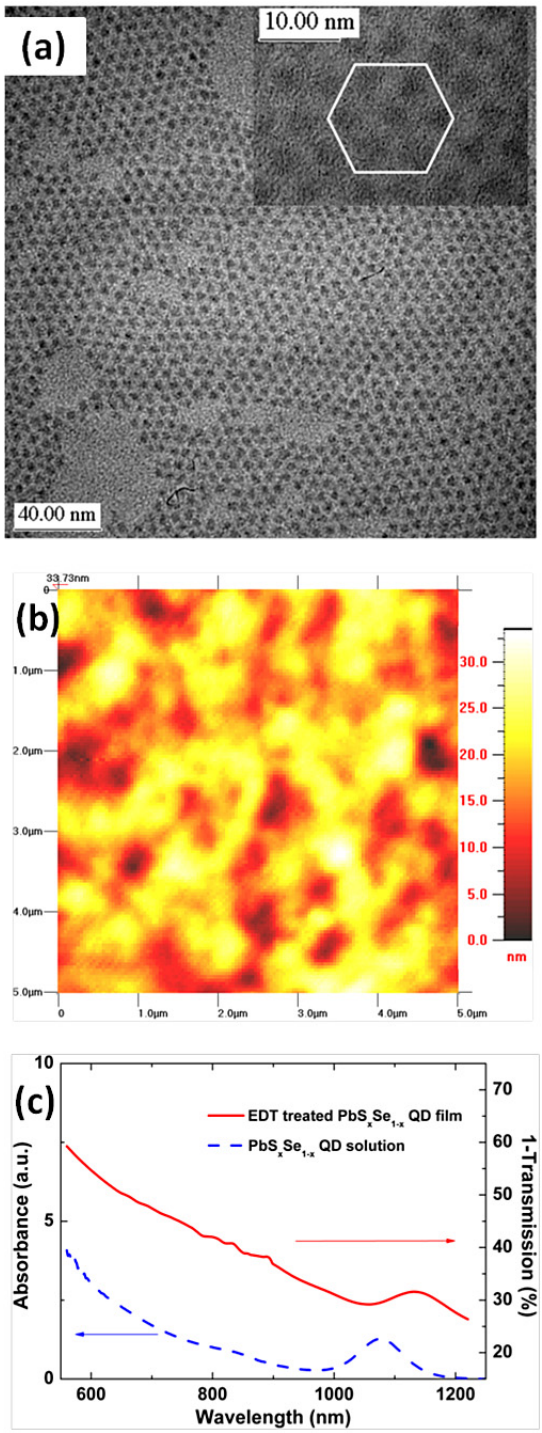

Figure 1. (a) TEM images of PbS_xSe_{1-x} QDs employed in this work. Inset: hexagonal array formed by self-assembly of ternary QDs. (b) An atomic force microscope topography image (5 μm $\times 5\mu$m) of a PbS_xSe_{1-x} QD film treated with EDT on a glass substrate. The root mean square (RMS) roughness of PbS_xSe_{1-x} QD film is 4 nm. (c) Optical absorption spectra of the PbS_xSe_{1-x} QDs in tetrachloroethylene solution (blue dashed line) and a spin-cast film with EDT treatment (red solid line).

films herein was determined from QD films deposited on glass substrates with the same spin-cast process as that for the devices. Considering the roughness of TiO_2 nanoparticle film (supporting information, figure S1 available at stacks.iop.org/Nano/23/405401/mmedia) and penetration of QDs into mesoporous TiO_2 film, as depicted in figure 2, the maximum 'actual' thickness of PbS_xSe_{1-x} QD films which photogenerated charge carriers might need to travel between the QD–Au interface and the QD–TiO_2 interface in devices may be up to 100 nm less than the measured PbS thickness. Here, for convenience we still use the thickness values obtained from QD films on glass to label them. Figure 3(a) shows the dependence of J_{sc} on PbS_xSe_{1-x} QD film thickness for such solar cells. The value of J_{sc} increases with QD film thickness initially, and then peaks when the film thickness reaches approximately 360 nm, which is near the thickness where the absorption reaches nearly 100% at a wavelength of 400 nm. As the thickness of QD film increases further, J_{sc} starts to decrease. Fill factors, as shown in figure 3(b), slightly reduce with increasing thickness of the $PbS_{0.9}Se_{0.1}$ QD film. Within our experimental error, V_{oc} remains unchanged on increasing the QD film thickness (see figure S2 available at stacks.iop.org/Nano/23/405401/mmedia). Therefore, the changes in the power conversion efficiency of devices with increasing QD film thickness (figure 3(b)) resembles the trend of J_{sc}.

For reasonable device performance, the photogenerated excitons must effectively dissociate, travel through the $PbS_{0.9}Se_{0.1}$ film, and be collected by electrodes within QD film and/or interfaces between QD film and electrodes (TiO_2 and Au), which is strongly affected by the thickness of QD film and quality of interfaces. As illustrated in figure 2(a), the rough surface of our mesoporous TiO_2 nanoparticle layer results in the formation of a quasi-bulk heterojunction region in the vicinity of the QD–TiO_2 interface, which would allow much more QDs loaded on TiO_2 film compared to a regular planar heterojunction structure and thereby facilitate the achievement of sufficient light absorption without sacrificing efficient dissociation, transportation and extraction of photogenerated charge carriers in devices. This benefit is similar to depleted bulk heterojunction PbS QD devices previously reported [23]; however, for our devices a tradeoff exists between light absorption and efficient carrier collection, as a bulk heterojunction structure is not formed throughout the whole active layer. We ascribe the increase of J_{sc} before the $PbS_{0.9}Se_{0.1}$ QD film reaches 360 nm thickness to additional excitons photoexcited in thicker films. The differences in the near-infrared region of the external quantum efficiency (EQE), shown for the 240 and 360 nm thick $PbS_{0.9}Se_{0.1}$ QD films in figure 4, support that the lower J_{sc} of thinner devices is limited by light absorption. The following decrease of J_{sc} with further increasing thickness of QD film is likely due to the recombination loss of charge carriers in too thick a QD film. The fill factor is a more complicated parameter compared to J_{sc} and V_{oc}, as it is affected by many factors. The reduction of fill factor with increasing QD film thickness observed in this work was also reported in titanium oxide/conjugated polymer photovoltaics with similar device configuration [19], which is induced by resistive loss of charge carriers in QD film. The increase of fill factors with lowering light intensity was also observed (figure S3 available at stacks.iop.org/Nano/23/405401/mmedia), indicating that the loss is

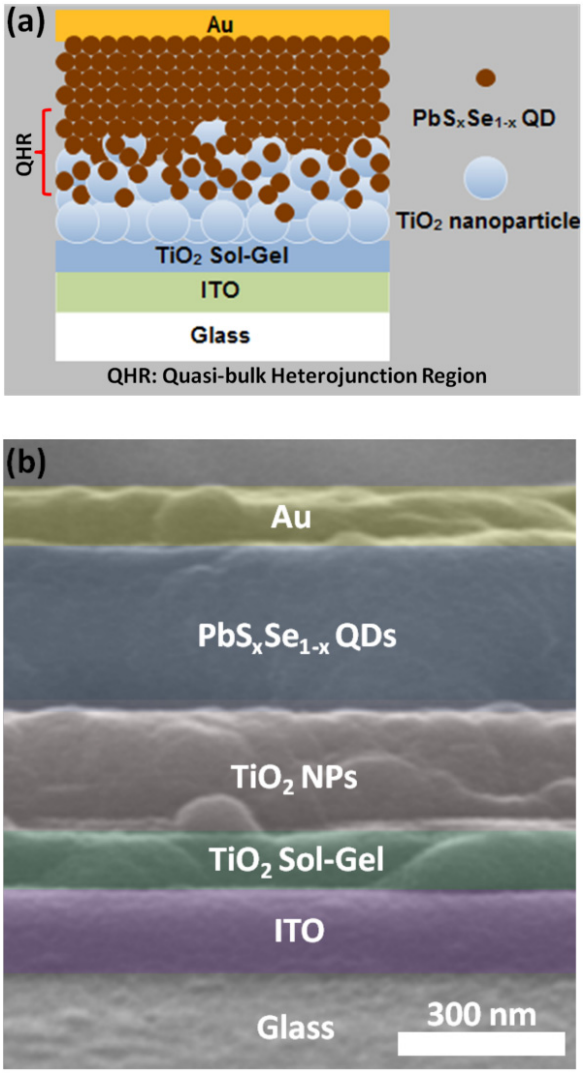

Figure 2. (a) Schematic of the PbS_xSe_{1-x} QD/TiO_2 heterojunction solar cell. Note that the thickness of each layer is not proportional to their actual thickness in real devices. The quasi-bulk heterojunction region is highlighted here. (b) Cross-sectional HR-SEM of the PbS_xSe_{1-x} QD/TiO_2 solar cell illustrated in (a).

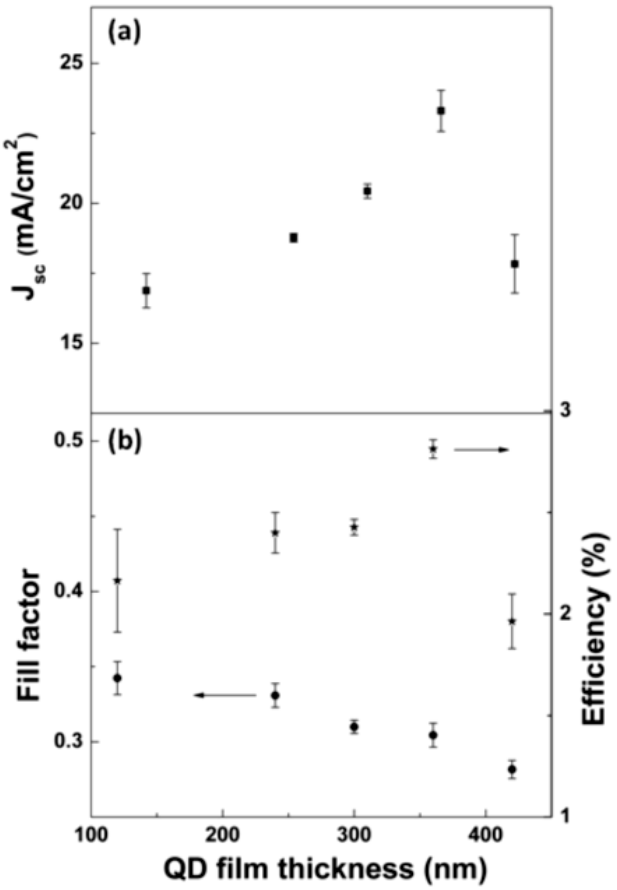

Figure 3. Dependence of J_{sc} (a), fill factor (b, circle) and energy conversion efficiency (b, star) on the thickness of the ternary PbS_xSe_{1-x} QD layer in TiO_2/PbS_xSe_{1-x} QD heterojunction solar cells. J_{sc}, fill factor and energy conversion efficiency values for devices with QD film thicknesses of 120 ± 10, 240 ± 20, 300 ± 25, 360 ± 30, and 420 ± 35 nm. The devices were measured after ~24 h aging in a nitrogen-filled glove box. Each data point corresponds to an average of all solar cells fabricated on the same substrate. The error bars for each data point represent one standard deviation of these devices.

less important at low intensities due to the direct relationship between the power and current flowing through a resistive layer [19].

The $PbS_{0.9}Se_{0.1}$ QD heterojunction solar cells stored in the dry nitrogen glove box showed improvements in V_{oc} and fill factor over days, without reduction in J_{sc}, reaching a maximum in 1–3 days of storage. A similar phenomenon exists in our heterojunction solar cells based on binary PbS QD treated with EDT [24], which also resembles the aging effects reported very recently in ZnO/PbSe QD devices, though treated with EDT + hydrazine instead of EDT only [18]. Unless stated otherwise, our data were taken after the initial rise in performance. Figure 5 shows the *J*–*V* characteristics of our best solar cell, which is composed of ~360 nm thick $PbS_{0.9}Se_{0.1}$ QD film. The solar cell exhibited a J_{sc} of 25.6 mA cm^{-2}, V_{oc} of 0.451 V, a fill factor of 36.8%, and an overall power conversion efficiency of 4.25% under illumination of 100 mW cm^{-2} simulated AM 1.5

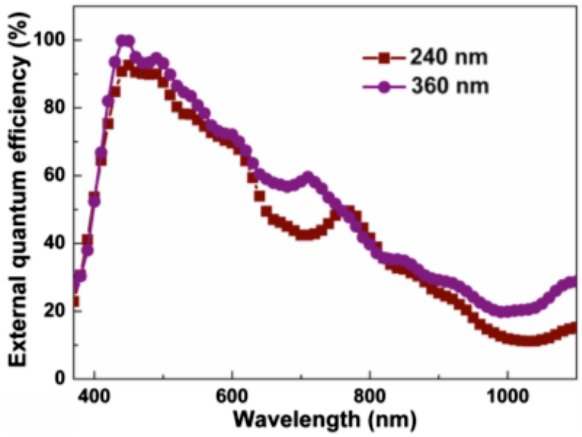

Figure 4. Dependence of EQE on PbS_xSe_{1-x} QD film thickness. Typical EQE curves for heterojunction solar cells with 240 ± 20 nm (circle) and 360 ± 30 nm (cubic) thick PbS_xSe_{1-x} QD films, respectively.

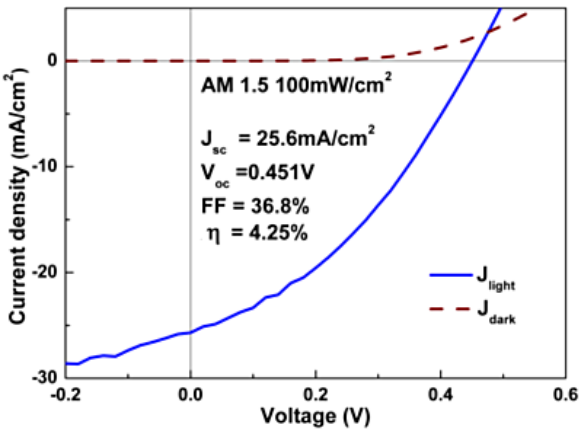

Figure 5. Current-density–voltage (J–V) characteristics of a TiO_2/PbS_xSe_{1-x} QD heterojunction solar cell with the best performance under 100 mW cm^{-2} simulated AM 1.5 illumination.

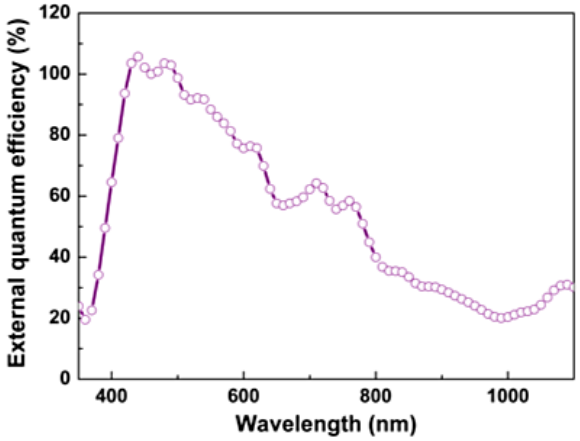

Figure 6. External quantum efficiency (EQE) curve of the ternary QD heterojunction solar cell characterized in figure 5.

light, which represents an ∼30% improvement of device performance compared to ternary $PbS_{0.9}Se_{0.1}$ QD Schottky junction devices reported previously [7]. The J_{sc} of such a ternary QD device is also much higher than that of our previous binary PbS QD device [25]. The EQE spectrum of a corresponding solar cell, as shown in figure 6, was measured from 350 to 1100 nm relative to that of a calibrated Si photodiode (Newport). Integrating the product of the EQE and the AM 1.5G spectrum from 350 to 1100 nm yields a J_{sc} of 24.1 mA cm^{-2}, which is in good agreement with that extracted from the J–V curve, given that the photocurrent contribution beyond 1100 nm is not accounted for. The device shows a peak EQE exceeding 100% (i.e. ∼105%) at 440 nm, indicating the existence of MEG-like behavior in $PbS_{0.9}Se_{0.1}$ QDs at much lower energies than have been previously reported [18]. However, the EQE of devices starts to drop with a further decrease of light wavelength, probably due to the gradually increased absorption and reflection of ITO glass and TiO_2 layers (see figure S4 available at stacks.iop.org/Nano/23/405401/mmedia). A significant interference peak at about 730 nm can also be seen in the EQE spectrum due to the built-up of optical modes in the dielectric stack of devices. As expected, the position of these interference peaks shifts with a change of PbS_xSe_{1-x} QD film thickness, as shown in figure 4.

We measured the EQE of same device with a new Thorlabs calibrated silicon photodiode and two diode lasers (447 and 405 nm) to check the accuracy of our EQE measurements shown above via the Newport calibrated silicon photodiode. As shown in figure 7(a), we obtained an EQE of 101 ± 4.6 % at 447 nm at different laser intensities, which agrees with the EQE spectrum above. The EQE of the device at 405 nm also shows agreement with the EQE spectrum (inset in figure 7(a)). The slight decrease in the EQE at 405 nm with increasing illumination intensity (>10 mW cm^{-2}) is probably due to the reduced recombination lifetime of charge carriers under stronger illumination [26]. All EQE <100% at different 405 nm laser intensity also confirms the observation in the EQE spectrum shown above that quantum efficiency is lower than 100% in the short-wavelength portion of the light spectrum (<440 nm), most likely caused by light loss in the ITO glass and TiO_2 layers. Enhanced interfacial recombination of charge carriers excited by these high-energy photons may also contribute to the drop in EQE [18]. A similar drop of EQE in the region of 400–500 nm was also observed in IV–VI QD devices with comparable structure by other groups, while their peak EQEs are much lower than 100% [23, 27–29]. In figure 7 (b), the performance of a $TiO_2/PbS_{0.9}Se_{0.1}$ QD heterojunction solar cell under 3.35 mW cm^{-2} 447 nm laser illumination is shown, with an energy conversion efficiency of 5.65%.

While our devices show high J_{sc} and V_{oc}, the performance is still limited by the lower fill factor. As shown in figure 5, the shunt resistance (estimated by the reciprocal of the slope of J–V curve at short circuit) is reduced significantly when the cell is illuminated compared to that in the dark. This so-called photoshunt effect, similar for the ZnO/PbSe QD devices [27], is one of the reasons for the low fill factor. Moreover, the crossing of J–V curves under illumination and in the dark is observed under forward bias in our devices, which is also thought to limit the fill factor and device performance [27, 30]. It has recently been reported that hydrazine + EDT treatment can eliminate the crossover [18]. If hydrazine was used as ligand together with EDT in ternary QD devices then a further improvement in energy conversion efficiency of $PbS_{0.9}Se_{0.1}$ QD devices might be expected.

In conclusion, we have fabricated heterojunction solar cells employing ternary $PbS_{0.9}Se_{0.1}$ QDs and a transparent TiO_2 layer. These devices show both high photocurrent and high open circuit voltage, which has proved a challenge for quantum dot solar cell devices. The best devices achieve an efficiency of up to 4.25%, showing the great potential of ternary QDs in the application of QD photovoltaic devices. In addition, EQE exceeding 100% at 2.7× the bandgap energy are achieved in these ternary QD heterojunction devices with EDT treatment only, providing evidence for the existence of MEG-like effects in $PbS_{0.9}Se_{0.1}$ QDs. These results demonstrate the benefits of the ternary system, which combines the higher V_{oc} typical of binary PbS quantum dots with the higher J_{sc} typical of binary PbSe quantum dots to optimize solar cell device performance.

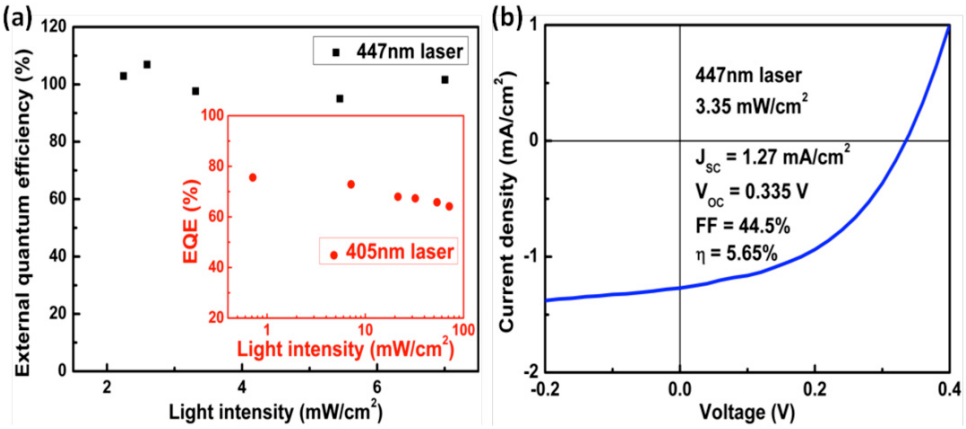

Figure 7. (a) External quantum efficiency (EQE) of corresponding PbS_xSe_{1-x} QD heterojunction device at different intensities of 447 nm laser light. Inset: external quantum efficiency (EQE) of the same device at different intensities of 405 nm laser light. (b) Current-density–voltage (J–V) characteristics of a TiO_2/PbS_xSe_{1-x} QD heterojunction solar cell under 3.35 mW cm^{-2} 447 nm laser illumination.

Acknowledgments

We thank Dr Campbell Scott at IBM Almaden Research Center and Dr Sanjay Tiwari at UCSC for help in measuring the optical parameters of TiO_2. We acknowledge support through the DOE SETP program (DOE DE-FG36-08GO18104) and the NSF Solar program (NSF DMR 1035478). GZ acknowledges the support of the China Scholarship Council.

References

[1] Wise F W 2000 Lead salt quantum dots: the limit of strong quantum confinement *Acc. Chem. Res.* **33** 773–80
[2] Schaller R D and Klimov V I 2004 High efficiency carrier multiplication in PbSe nanocrystals: implications for solar energy conversion *Phys. Rev. Lett.* **92** 186601
[3] Ellingson R J, Beard M C, Johnson J C, Yu P R, Micic O I, Nozik A J, Shabaev A and Efros A L 2005 Highly efficient multiple exciton generation in colloidal PbSe and PbS quantum dots *Nano Lett.* **5** 865–71
[4] Hillhouse H W and Beard M C 2009 Solar cells from colloidal nanocrystals: fundamentals, materials, devices, and economics *Curr. Opin. Colloid Interface Sci.* **14** 245–59
[5] Debnath R, Bakr O and Sargent E H 2011 Solution-processed colloidal quantum dot photovoltaics: a perspective *Energy Environ. Sci.* **4** 4870–81
[6] Emin S, Singh S P, Han L, Satoh N and Islam A 2011 Colloidal quantum dot solar cells *Sol. Energy* **85** 1264–82
[7] Ma W, Luther J M, Zheng H, Wu Y and Alivisatos A P 2009 Photovoltaic devices employing ternary PbS_xSe_{1-x} nanocrystals *Nano Lett.* **9** 1699–703
[8] Yu K J *et al* 2011 Low-temperature noninjection approach to homogeneously-alloyed $PbSe_xS_{1-x}$ colloidal nanocrystals for photovoltaic applications *ACS Appl. Mater. Interfaces* **3** 1511–20
[9] Tang J and Sargent E H 2010 Infrared colloidal quantum dots for photovoltaics: fundamentals and recent progress *Adv. Mater.* **23** 12–29
[10] Nelson J 2003 *The Physics of Solar Cells* (London: Imperial College Press)
[11] Nair G, Geyer S M, Chang L-Y and Bawendi M G 2008 Carrier multiplication yields in PbS and PbSe nanocrystals measured by transient photoluminescence *Phys. Rev.* B **78** 125325
[12] Luther J M, Beard M C, Song Q, Law M, Ellingson R J and Nozik A J 2007 Multiple exciton generation in films of electronically coupled PbSe quantum dots *Nano Lett.* **7** 1779–84
[13] Beard M C, Midgett A G, Law M, Semonin O E, Ellingson R J and Nozik A J 2009 Variations in the quantum efficiency of multiple exciton generation for a series of chemically treated PbSe nanocrystal films *Nano Lett.* **9** 836–45
[14] Alerts M, Suchand Sandeep C S, Gao Y, Savenije T J, Schins J M, Houtepen A J, Kinge S and Siebbeles L D A 2011 Free charges produced by carrier multiplication in strongly coupled PbSe quantum dot films *Nano Lett.* **11** 4485–9
[15] Sambur J B, Novet T and Parkinson B A 2010 Multiple exciton collection in a sensitized photovoltaic system *Science* **330** 63–6
[16] Zhai G, Bezryadina A, Breeze A J, Zhang D, Alers G B and Carter S A 2011 Air stability of TiO_2/PbS colloidal nanoparticle solar cells and its impact on power efficiency *Appl. Phys. Lett.* **99** 063512
[17] Luther J M, Law M, Beard M C, Song Q, Reese M O, Ellingson R J and Nozik A J 2008 Schottky solar cells based on colloidal nanocrystal films *Nano Lett.* **8** 3488–92
[18] Semonin O E, Luther J M, Choi S, Chen H-Y, Gao J, Nozik A J and Beard M C 2011 Peak external photocurrent quantum efficiency exceeding 100% via MEG in a quantum dot solar cell *Science* **334** 1530–3
[19] Arango A C, Johnson L R, Bliznyuk V N, Schlesinger Z, Carter S A and Hörhold H-H 2000 Efficient titanium oxide/conjugated polymer photovoltaics for solar energy conversion *Adv. Mater.* **12** 1689–92
[20] Luther J M, Law M, Song Q, Perkins C L, Beard M C and Nozik A J 2008 Structural, optical, and electrical properties of self-assembled films of PbSe nanocrystals treated with 1,2-ethanedithiol *ACS Nano* **2** 271–80
[21] Cademartiri L, Montanari E, Calestani G, Migliori A, Guagliardi A and Ozin G 2006 Size dependent extinction coefficients of PbS quantum dots *J. Am. Chem. Soc.* **128** 10337–46
[22] Moreels I, Lambert K, Muynck D D, Vanhaecke F, Poelman D, Martins J C, Allan G and Hens Z 2007 Composition and size-dependent extinction coefficient of colloidal PbSe quantum dots *Chem. Mater.* **19** 6101–6

[23] Barkhouse D A R, Debnath R, Kramer I J, Zhitomirsky D, Pattantyus-Abraham A G, Levina L, Etgar L, Grätzel M and Sargent E H 2011 Depleted bulk heterojunction colloidal quantum dot photovoltaics *Adv. Mater.* **23** 3134–8

[24] Zhai G, Breeze A, Graham R, France C, Bezryadina A, Alers G B and Carter S A 2010 Effect of air exposure on performance of PbS/TiO_2 heterojunction colloidal quantum dot solar cells *MRS Photovoltaic Workshop (Denver, CO)*

[25] Ju T, Graham R L, Zhai G, Rodrigues Y W, Breeze A J, Yang L, Alers G B and Carter S A 2010 High efficiency mesoporous titanium oxide PbS quantum dot solar cells at low temperature *Appl. Phys. Lett.* **97** 043106

[26] Koleilat G I, Levina L, Shukla H, Myrskog S H, Hinds S, Pattantyus-Abraham A G and Sargent E H 2008 Efficient, stable infrared photovoltaics based on solution-cast colloidal quantum dots *ACS Nano* **2** 833–40

[27] Leschkies K S, Beatty T J, Kang M S, Norris D J and Aydil E S 2009 Solar cells based on junctions between colloidal PbSe nanocrystals and thin ZnO films *ACS Nano* **3** 3638–48

[28] Debnath R, Greiner M T, Kramer I J, Fischer A, Tang J, Barkhouse D A R, Wang X, Levina L, Lu Z-H and Sargent E H 2010 Depleted-heterojunction colloidal quantum dot photovoltaics employing low-cost electrical contacts *Appl. Phys. Lett.* **97** 023109

[29] Gao J, Luther J M, Semonin O E, Ellingson R J, Nozik A J and Beard M C 2011 Quantum dot size dependent *J–V* characteristics in heterojunction ZnO/PbS quantum dot solar cells *Nano Lett.* **11** 1002–8

[30] Choi J J *et al* 2009 PbSe nanocrystal excitonic solar cells *Nano Lett.* **9** 3749–55